JOURNAL OF GEOPHYSICAL RESEARCH, VOL. 93, NO. B4, PAGES 3232-3242, APRIL 10, 1988

Using Surface Displacement and Strain Observations to Determine Deformation at Depth, With an Application to Long Valley Caldera, California

D. W. VASCO,[1,2] L. R. JOHNSON,[1] AND N. E. GOLDSTEIN

Center for Computational Seismology, Earth Sciences Division, Lawrence Berkeley Laboratory University of California, Berkeley

We present a method for the inversion of surface displacement and strain to determine six independent combinations of the strain components at depth. These six combinations represent three mutually perpendicular double forces without moment and three pairs of double forces with moment. Furthermore, they may be directly related to a moment tensor density distribution for static strain. The method is linear and, unlike other methods, does not depend on an a priori source model. Due to the linearity of the formulation, methods such as generalized inversion or l^1 residual norm minimization may be used to determine models of deformation at depth. The methods presented are applicable to a variety of available geodetic data sets. The technique is applied to repeat leveling data taken between 1982 and 1985 in Long Valley caldera. We determined a model of the magma intrusion suspected to have occurred beneath the caldera. The model derived minimized the l^2 norm of the difference between the predicted and observed data subject to the constraint that only intrusion occur. The model indicates that most volume expansion took place in the caldera region above 8 km $\pm$ 2 km. In the 0–4 km depth range the expansion is widely distributed with a maximum value of 0.005 km^3. Deeper, 4–8 km, there is a concentration of intrusion in the central portion of the caldera. The maximum volume increase here is 0.030 km^3.

INTRODUCTION

Many methods have been proposed to determine subsurface deformation, such as fault shear, from surface displacement observations. Unfortunately, most methods rely on local linearization about some assumed source geometry. Because of this, these methods are dependent on the type of model assumed. If the form of this model is not general enough to include all possible source types or multiple sources, then the results may be misleading. *Dieterich and Decker* [1975] have illustrated the ambiguity caused by variations in source shape. Considering a variety of volume sources fitting the same vertical uplift data, these authors note that source depths varied by a factor of 3.5.

In this paper we present a stable, systematic method for the inversion of surface displacement and strain to obtain a measure of deformation at depth without the need of assuming an initial source model. To do this, we examine the problem in terms of certain combinations of the tensor components of strain at depth. The deformation is characterized by the three-dimensional distribution of six linear combinations of strain components. The distribution is discretized using a series expansion method, and a linear inverse problem is presented without local linearization. The linearity is an important feature of the method because it allows one to compute the data resolution matrix, the parameter resolution matrix, and the parameter covariance matrix [*Menke*, 1984]. The basis functions for the series can be general enough to include all source types. This inverse problem may then be solved by minimizing the difference between the predicted data and the observed data in an l^1 or l^2 (least squares) sense. Unfortunately, for each term of the series expansion, six unknowns are involved. For a reasonable order of expansion this usually results in an underdetermined inverse problem. Consequently, it is often advisable to use an extremal inversion technique to derive bounds on model parameters [*Langbein*, 1981; *Vasco and Johnson*, 1985]. The methods presented in this paper are also applicable to a wide variety of other geodetic data sets, such as the recent set of Global Positioning System (GPS) measurements and the repetitive trilateration observations being made at Parkfield, California. This approach is a generalization of methods such as those presented by *Langbein* [1981], *Ward and Barrientos* [1986], and *Segall and Harris* [1987]. We consider the three-dimensional distribution of the moment tensor density rather than the distribution of the scalar moment on a fault surface. This allows one to consider more general sources, such as dike injection, in a fully linear fashion.

RELATIONSHIP BETWEEN DISPLACEMENT AT DEPTH AND DISPLACEMENT AT THE SURFACE

Inferences about internal Earth movements, such as due to faulting and magma injection, must often be made solely from surface displacement measurements. The displacements at the Earth's surface, $u_m(\mathbf{x})$, are related to a dislocation distribution, $\Delta u_k(\xi)$, on an internal dislocation surface Σ by the Volterra integral [*Volterra*, 1907; *Aki and Richards*, 1980*a*],

$$u_m(\mathbf{x}) = \int_\Sigma \Delta u_k(\xi) W_m^{kl}(\mathbf{x}, \xi) v_l \, d\Sigma \qquad (1)$$

where $\mathbf{x} = (x_1, x_2, x_3)$ is any point in the half-space other than the dislocation surface itself and $\xi = (\xi_1, \xi_2, \xi_3)$ is a point on the dislocation surface. $W_m^{kl}(\mathbf{x}, \xi)$ is the Green function relating the dislocation $\Delta u_k(\xi)$ to the surface displacement component $u_m(\mathbf{x})$. The parameter v_l is the lth component of the normal to the surface Σ. In this article the summation convention is assumed.

[1]Also at Department of Geology and Geophysics, University of California, Berkeley.

[2]Now at Earth Sciences Division, Air Force Geophysics Laboratory, Hanscom Air Force Base, Massachusetts.

Paper number 7B2033.
0148-0227/88/007B-2033$05.00

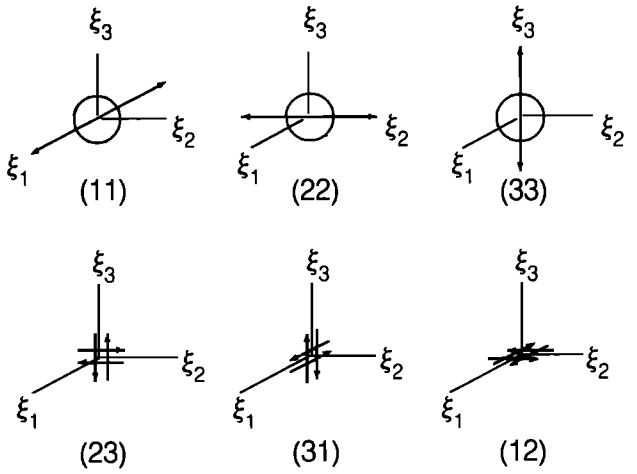

Fig. 1. The six canonical source types giving rise to the displacements $W_m^{kl}(\mathbf{x}, \xi)$. The diagonal terms represent vector dipoles along the successive axes plus a center of dilation. The off-diagonal (ij) terms are double couples in the (ξ_i, ξ_j) plane.

The Green function in equation (1), $W_m^{kl}(\mathbf{x}, \xi)$, may be written in terms of the spatial derivatives with respect to the source coordinates of the displacement field U_m^k [*Maruyama*, 1964],

$$W_m^{kl}(\mathbf{x}, \xi) = -\lambda\delta_{kl}U_m^{n,n} - \mu(U_m^{k,l} + U_m^{l,k}) \tag{2}$$

Here $U_m^{k,l}$ represents $\partial U_m^k/\partial\xi_l$, λ and μ are Lame's constants, and δ_{kl} in the Kronecker delta. U_m^k represents the mth component of displacement due to a unit body force in the x_k direction, and $U_m^{k,l}$ can be interpreted as the mth component of displacement at the surface point $\mathbf{x}$ generated by two opposite forces in the kth direction of equal magnitude $1/\Delta x_l$, at a distance Δx_l apart, acting at the source point ξ. If $k = l$, this nucleus of strain is known as a double force without moment. In this case it may be seen from equation (2) that $W_m^{kl}(\mathbf{x}, \xi)$ is a combination of a center of dilation and a double force in the kth direction. Similarly, for $k \neq l$ is the sum of two coplanar, perpendicular double forces with moment. The six possible force combinations are shown in Figure 1.

The point force combinations at ξ causing the displacement at a point $\mathbf{x}$ on the surface has a representation as a combination of the six double forces shown in Figure 1. Hence the displacement at $\mathbf{x}$ due to a distribution of dislocations at depth may be written

$$u_m(\mathbf{x}) = \int_V \varepsilon_{kl}(\xi)W_m^{kl}(\mathbf{x}, \xi)\, dV(\xi) \tag{3}$$

where $\varepsilon_{kl}(\xi)$ may be considered as a weighting function of the double forces at source point ξ. Because of the symmetry of $W_m^{kl}(\mathbf{x}, \xi)$ only six independent values exist. By differentiating equation (3) with respect to the station coordinates one may derive a relationship between the strain at the surface and the six double strain nuclei. The expressions for $W_m^{kl}(\mathbf{x}, \xi)$ for a half-space with a Poisson's ratio of 0.25 are given by *Maruyama* [1964]. They are given in the appendix for a half-space with an arbitrary Poisson's ratio. Other methods exist for the computation of $W_m^{kl}(\mathbf{x}, \xi)$ in a layered half-space [*Jovanovich et al.*, 1974] and in a half-space with an arbitrary distribution of Poisson's ratio [*Dieterich and Decker*, 1975]. A representation of the Volterra integral in terms of a volume integral such as equation (3) is derived by *Vasco* [1986].

The importance of the representation in equation (3) is that it is linear and that it may be interpreted in terms of the six canonical source types shown in Figure 1. This interpretation will allow the determination of the distribution of principal strains and principal strain axes, as will be shown in a later section. This representation is similar to the moment tensor representation used in seismic source theory. In fact, a direct connection exists between the tensor distribution $\varepsilon_{kl}(\xi)$ and the moment tensor density distribution for static strain. The moment tensor density $m_{kl}(\xi)$ is a tensor-valued function from which the equivalent body forces may be derived,

$$\mathbf{f}(\xi) = -\nabla \cdot \mathbf{m}(\xi)$$

Here $\mathbf{f}(\xi)$ is a body force distribution which gives the same surface deformation as the true source. From the discussion following equation (2) it is seen that the displacement at the surface due to a general body force distribution is given by

$$u_m(\mathbf{x}) = \int_V U_m^k(\mathbf{x}, \xi)f_k(\xi)\, dV(\xi)$$

Integrating this expression by parts, one finds that

$$u_m(\mathbf{x}) = \int_V U_m^{k,l}(\mathbf{x}, \xi)m_{kl}(\xi)\, dV(\xi)$$

To show the relationship between $m_{kl}(\xi)$ and $\varepsilon_{kl}(\xi)$, substitute equation (2) into equation (3), and after rearranging terms we find that

$$u_m(\mathbf{x}) = \int_V U_m^{k,l}(\mathbf{x}, \xi)\{-\lambda\delta_{kl}\varepsilon_{ii}(\xi) - \mu[\varepsilon_{kl}(\xi) + \varepsilon_{lk}(\xi)]\}\, dV(\xi)$$

Comparing this expression with that for displacement due to the moment tensor density $m_{kl}(\xi)$, it is seen that

$$m_{kl}(\xi) = -\lambda\varepsilon_{ii}\delta_{kl}(\xi) - \mu[\varepsilon_{kl}(\xi) + \varepsilon_{lk}(\xi)]$$

With the exception of a sign change, this is the same as the relationship between the seismic moment tensor density and the inelastic strain in the source region [*Madariaga*, 1983]. The relationship is clarified by the following thought experiment [*Eshelby*, 1957]: Remove an infinitesimal volume from the source volume V and allow it to undergo an inelastic strain $\varepsilon_{kl}(\xi)$. Apply the stresses on the surface of the volume necessary to bring the volume back to its initial shape. As is seen above, these stresses are given by the moment tensor if the elastic constants have not changed. Therefore the moment tensor density represents the internal stresses needed to cancel the stresses produced by inelastic strains at the source. The difference in sign is due to the fact that the moment tensor is the stress canceling the strain, not the stress giving rise to the strain. The above relationship may be used to compare geodetically derived moment tensors with seismologically derived moment tensors. We wish to emphasize that the description is of an equivalent source and not of the true physical source. The actual physical mechanisms of a source are very complicated, involving lateral heterogeneity of mechanical properties along with large and probably nonlinear strains. Therefore an equivalent source representation is used in order to determine the linear elastic features of the source.

The linearity of the above formulation simplifies questions involving uniqueness and resolution because methods to determine these properties for linear inverse problems are well established in geophysics. Before discussing this, however, the problem will be discretized for the sake of later computation.

DISCRETIZATION OF THE MODEL

In this section we discretize the inverse problem through a series expansion method. It is at this stage that the problem of source representation is addressed. As mentioned above, previous methods have tended to choose a particular source model specified by a finite number of parameters. The model parameters are then determined such that the predicted deformation and observed deformation match. Another possibility, one presented here, is to expand the strain nuclei distribution in a three-dimensional orthonormal series. This is advantageous in that the data still depend linearly on the parameters. Furthermore, the basis functions can be general enough to represent all possible sources. Finally, because of the orthogonality of the series the estimate of each term in the expansion is independent of the number of terms used in the representation.

First, a set of N orthonormal basis functions $\beta_j(\xi)$, $j = 1, \cdots, N$ is introduced. The model space is now restricted to those six model parameter distributions $\varepsilon_{kl}(\xi)$ which may be described as a linear combination of the N basis functions,

$$\varepsilon_{kl}(\xi) = \sum_{j=1}^{N} b_{kl}{}^{j}\beta_j(\xi)$$

The problem becomes one of determining the coefficients of the expansion $b_{kl}{}^{j}$ such that the model is compatible with the data. Rewriting equation (3) using the series expansion given above and suppressing the summation convention,

$$u_m(\mathbf{x}) = \int_V \sum_{j=1}^{N} \sum_{kl} b_{kl}{}^{j}\beta_j(\xi) W_m{}^{kl}(\mathbf{x}, \xi)\, dV(\xi)$$

The sum over the kl pairs includes only six terms, (11), (12), (13), (22), (23), (33), because of the symmetry of $\varepsilon_{kl}(\xi)$. Defining

$$G_{jm}{}^{kl}(\mathbf{x}) = \int_V \beta_j(\xi) W_m{}^{kl}(\mathbf{x}, \xi)\, dV(\xi)$$

results in

$$u_m(\mathbf{x}) = \sum_{j=1}^{N} \sum_{kl} b_{kl}{}^{j} G_{jm}{}^{kl}(\mathbf{x})$$

Rewriting the sum over the three indices as a single sum from 1 to $6 \times N$,

$$u_m(\mathbf{x}) = \sum_{I=1}^{6\times N} b_I G_m{}^{I} \tag{4}$$

or, in matrix form,

$$\mathbf{u} = \mathbf{G}\mathbf{b}$$

a set of M linear equations for the $6 \times N$ unknown parameters $b_{kl}{}^{j}$. M is the number of station components used. A commonly used set of basis functions are the rectangular constant basis functions,

$$\begin{aligned} \beta_j(\xi) &= 1 \qquad \xi \text{ in } R_j \\ \beta_j(\xi) &= 0 \qquad \xi \text{ not in } R_j \end{aligned} \tag{5}$$

where R_j is the jth rectangle or block. For such basis functions, $G_{jm}{}^{kl}(\mathbf{x})$ is the average of $W_m{}^{kl}(\mathbf{x}, \xi)$ over R_j; $b_{kl}{}^{j}$ is the average perturbation of cell j.

An alternative set of basis functions are the Fourier wave functions,

$$\beta_j(\xi) = e^{iJ_1\xi_1} e^{iJ_2\xi_2} e^{iJ_3\xi_3}$$

where j is now a vector-valued index, $j = (J_1, J_2, J_3)$. These are useful when constraints are available on the amplitudes of the strain nuclei as a function of wave number.

The choice of basis functions and the number of terms needed in the series expansion depends on the geometry of the problem and the parameters of interest. In its full generality this approach may result in a large number of parameters. However, it is usually possible to reduce the number of parameters by incorporating a priori information when choosing the basis functions. For example, if the location and shape of a fault zone are known through seismicity studies, then only the two-dimensional fault plane need be considered. In another case, if only a volume change is postulated as a source, then only the terms in the expansion for which $k = l$ are used.

The resulting linear system of equations (4) may be solved by any of the methods commonly used in geophysics. In the next section the generalized inverse is presented. It allows efficient calculation of the parameter resolution and the variance of the solution. Last, it may be noted that it is not necessary to discretize the strain nuclei distribution $\varepsilon_{kl}(\xi)$. There are methods [*Backus and Gilbert*, 1968; *Tarantola and Valette*, 1982] which estimate continuous distributions of parameters from a finite number of observations.

THE l^2 MINIMUM RESIDUAL NORM SOLUTION

What is commonly referred to as the solution of equation (4) is that model which makes the sum of the squares of the differences between the predicted and observed data a minimum. As will be seen later, this is not the only possible solution to the system of equations (4).

One of the most used techniques in geophysics for the calculation of the minimum l^2 residual norm solution of equation (4) is the generalized inverse [*Wiggins*, 1972; *Aki and Richards*, 1980*b*]. It follows from the singular value decomposition of $\mathbf{G}$, the matrix in equation (4),

$$\mathbf{G} = \mathbf{U}\mathbf{\Lambda}\mathbf{V}^T \tag{6}$$

For p nonzero eigenvalues $\mathbf{U}$ is an M by p matrix consisting of the eigenvectors associated with the nonzero eigenvalues of $\mathbf{G}\mathbf{G}^T$. $\mathbf{V}^T$ is the transpose of a $6N$ by p matrix of eigenvectors of $\mathbf{G}^T\mathbf{G}$, and $\mathbf{\Lambda}$ is a $p \times p$ diagonal matrix of the nonzero singular values of $\mathbf{G}^T\mathbf{G}$. The generalized inverse is written in terms of the singular value decomposition

$$\mathbf{G}^{-1} = \mathbf{V}\mathbf{\Lambda}^{-1}\mathbf{U}^T \tag{7}$$

and the estimate of the solution is given as

$$\mathfrak{b} = \mathbf{V}\mathbf{\Lambda}^{-1}\mathbf{U}^T\mathbf{u} \tag{8}$$

The advantage of the singular value decomposition, justifying the extra computational effort, is that instabilities in the inverse can be eliminated by not considering the small eigenvalues. Also, the decomposition makes clear which parameters are well determined and which data are important. The resolution matrix, that is, the matrix $\mathbf{R}$ which relates the estimate of the parameters to their true values,

$$\mathfrak{b} = \mathbf{R}\mathbf{b}$$

is readily written in terms of the singular value decomposition,

$$\mathbf{R} = \mathbf{V}\mathbf{V}^T \tag{9}$$

The covariance matrix of the model parameters, $\mathbf{C}_{bb}$, which represents an estimate of the error in the solution, can be related to the data covariance matrix, $\mathbf{C}_{uu}$,

$$\mathbf{C}_{bb} = \mathbf{V}\Lambda^{-1}\mathbf{U}^T\mathbf{C}_{uu}\mathbf{U}\Lambda^{-1}\mathbf{V}^T \tag{10}$$

Once a model $\mathbf{b}$ has been determined, estimates are available of the six independent source components distributed in the subsurface. If the rectangular constant basis functions of equation (5) are used, then each set of elements (b_{kl}^j, $kl = 11, 12, 13, 22, 23, 33$) represents the six strain combinations for the jth block. These may be written as a symmetric three by three matrix,

$$\mathbf{B}^j = \begin{pmatrix} b_{11}^j & b_{21}^j & b_{31}^j \\ b_{21}^j & b_{22}^j & b_{32}^j \\ b_{31}^j & b_{32}^j & b_{33}^j \end{pmatrix} \tag{11}$$

The diagonal terms represent the double strains without moment, and the off-diagonal terms represent the shear double couples. By decomposing the $\mathbf{B}^j$ matrix,

$$\mathbf{B}^j = \mathbf{W}^j\Phi^j\mathbf{W}^{jT} \tag{12}$$

it is possible to derive the principal strains, the diagonal elements of Φ^j, and the principal directions $\mathbf{w}^j$, the column vectors of $\mathbf{W}^j$, for the jth block. Thus surface strain and displacement measurements may be used to determine the three-dimensional distribution of strain.

It is easy to include the requirement that no net volume change occurs in the jth block by setting the sum of the diagonal terms in equation (11) to zero,

$$b_{11}^j + b_{22}^j + b_{33}^j = 0 \tag{13}$$

A variety of other linear constraints are possible such as restricting the problem to horizontal shear strains. Efficient methods are available for solving the linear least squares problem subject to inequality constraints [*Lawson and Hanson*, 1974]. Also, because of the many unknowns associated with each block, the problem may be highly underdetermined. In such a case the generalized inverse will return the solution with the smallest l^2 norm. Perhaps extremal inversion, which derives bounds on model parameters rather than the parameter values themselves, is better suited for treating such cases.

As an application of the methods presented, consider the example shown in Figures 2*a* and 2*b*. Two infinitely long strike-slip faults undergo slip perpendicular to the plane of Figure 2, giving rise to the horizontal displacement shown in Figure 2*b*. The faults, located within the centers of the shaded regions in Figure 2*a*, undergo slip of 1.0 and 1.5 (solid pattern). The region is discretized into 100 blocks, each of which may undergo horizontal slip in the same direction as the slip of the fault. Note that if the exact fault geometry had been known, the number of unknowns could be reduced from 100 to 7 in this example. By applying the algorithm presented in this section to the displacements recorded at 100 stations, the distribution of slip in the subsurface may be derived (Figure 3). With no a priori fault model the locations of the two faults are resolved, as is the relative vertical extent of each fault. The slip in this model is somewhat distributed around the fault plane, tending toward larger values near the surface. The concentration at the surface is due to the fact that the tails of the surface displacement distributions were not sampled. The concentration is also due to the above mentioned tendency of the generalized inverse to produce the minimum norm solution for underdetermined problems.

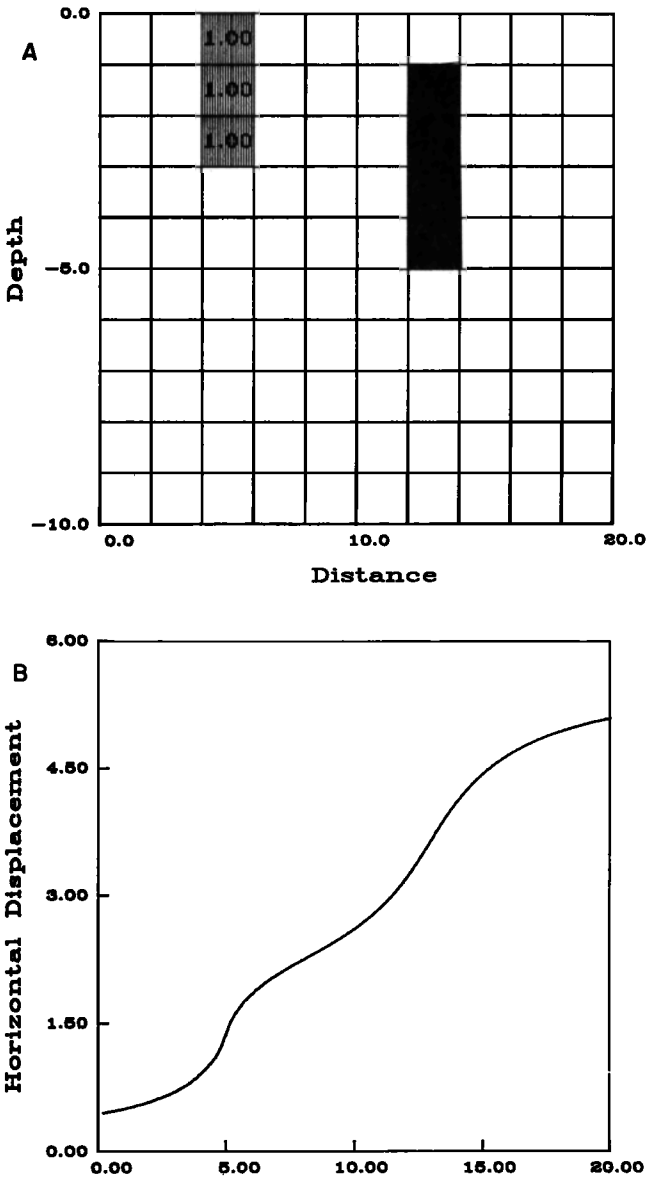

Fig. 2. (*a*) Two-dimensional model of horizontal fault slip. The faults are vertical, lying in the center of the shaded columns of blocks. They have undergone 1.0 and 1.5 (solid) percent of slip relative to the distance scale. (*b*) Horizontal displacement, in percent of the distance scale, associated with the source model.

The l^1 Residual Norm Minimization

The least squares or l^2 solution is only one of many possible models which may be derived from the data. One alternative, which may be advantageous in some problems, is to compute a solution that results in the minimization of the l^1 norm of the residuals. This is the minimization of the sum of the absolute values of the predicted data minus the observed data,

$$\| \mathbf{u} - \mathbf{G}\mathbf{b} \|_1 = \sum_{i=1}^{M} \left| \sum_{j=1}^{N} u_i - G_{ij}b_j \right|$$

possibly subject to equality or inequality constraints. In this approach, where we seek a single model, we can formulate the

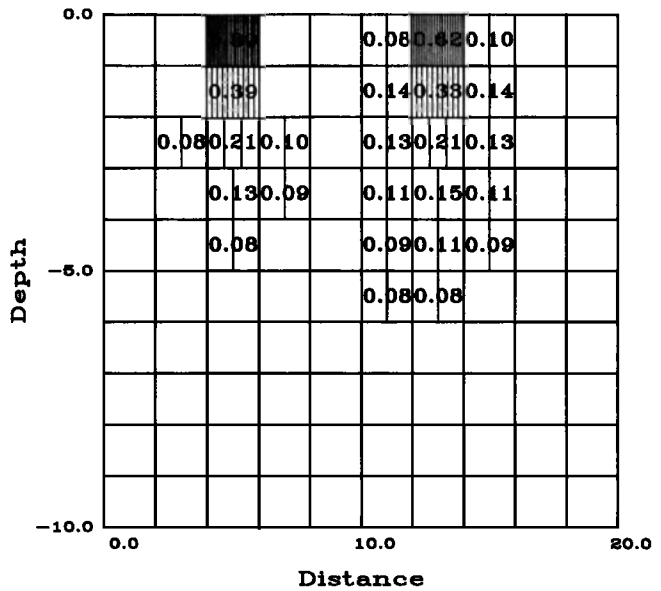

Fig. 3. Result of a least squares minimization of the residuals. The data inverted to generate this model were shown in Figure 2.

problem as a minimization problem subject to equality and inequality constraints,

$$\min \sum_i x_i + \tilde{x}_i$$

subject to

$$(\mathbf{G} \quad \mathbf{I} \quad -\mathbf{I}) \begin{pmatrix} \mathbf{b} \\ \mathbf{x} \\ \tilde{\mathbf{x}} \end{pmatrix} = \mathbf{u}$$

$$\mathbf{b} \geq 0 \qquad \mathbf{x} \geq 0 \qquad \tilde{\mathbf{x}} \geq 0$$

The $\mathbf{x}$ and $\tilde{\mathbf{x}}$ are dummy vectors which may take any nonnegative value. Linear optimization problems subject to linear equality and inequality constraints, such as presented in above, are easily solved using linear programming techniques [*Hadley*, 1962]. The simplex method, the standard solution algorithm [*Dantzig*, 1963], is very efficient and can solve problems of the order of thousands of variables and thousands of constraints.

As with the generalized inverse solution, by diagonalizing the matrix of coefficients b_j^{kl} shown in equation (11), the principal strains and the principal directions of strain may be determined. Because the problem may be formulated as a linear programming problem, it is now easy to include inequality constraints such as specifying that only volume expansion occurs. Also the l^1 residual norm minimization solution is less sensitive to large blunders in the data; that is, a few random large errors will not produce large changes in the model. As noted by *Savage et al.* [1986], trilateration data may contain such errors.

Constraints on Volume Change

A problem which arises in active volcanic regions is to determine the location of an expanding or ascending magma body on the basis of a set of surface deformation and strain observations. This is an inherently nonunique inverse problem which has often been treated by fitting a prescribed source model to the data. We feel that a better approach is the one give above, adapted for the particular case of volume expansion. Because this problem was treated in another work [*Vasco and Johnson*, 1985] it will only be outlined as a connection between the general method already presented and the application given in the next section.

Consider the volume integral in equation (3). For a volume dilatational source $kl = 11, 22, 33$, this integral reduces to

$$u_m(\mathbf{x}) = \int_V \varepsilon_{kk}(\xi) W_m^{kk}(\mathbf{x}, \xi)\, dV \tag{14}$$

For a fluid source volume,

$$\varepsilon_{11}(\xi) = \varepsilon_{22}(\xi) = \varepsilon_{33}(\xi) = \Delta\theta(\xi)$$

$\Delta\theta(\xi)$ is the fractional volume change defined by $\Delta V/V^0$, where ΔV is the change in volume and V^0 is the initial volume of the fluid body. Furthermore, if we define

$$K_m(\mathbf{x}, \xi) \equiv W_m^{11}(\mathbf{x}, \xi) + W_m^{22}(\mathbf{x}, \xi) + W_m^{3}(\mathbf{x}, \xi)$$

then by using the expressions for $W_m^{kk}(\mathbf{x}, \xi)$ given in the appendix, $K_m(\mathbf{x}, \xi)$ may be written as

$$K_m(\mathbf{x}, \xi) = \frac{1}{3\pi}(\nu + 1)\frac{x_m - \xi_m}{S^3}$$

where

$$S = [(x_1{}^i - \xi_1)^2 + (x_2{}^i - \xi_2)^2 + \xi_3{}^2]^{1/2}$$

ν is Poisson's ratio and $x_3 = 0$. Therefore the displacement in equation (14) can be written in terms of a scalar volume change, $\Delta\theta$,

$$u_m(\mathbf{x}) = \int_V \Delta\theta(\xi) K_m(\mathbf{x}, \xi)\, dV \tag{15}$$

This is the standard form of a scalar linear inverse problem.

Using equation (15), it is possible to formulate a method to compute volume change models. In the next section, such a model will be derived for an expanding magma body giving rise to the observed uplift in Long Valley caldera, California.

Model of Volume Expansion in Long Valley Caldera, California

During the 10-year interval 1975–1985, up to 47 cm of vertical displacement were measured within Long Valley caldera (Figure 4) [*Savage and Clark*, 1982; *Castle et al.*, 1984]. Four surveys from this period are shown in Figures 5 and 6, those made in 1982, 1983, 1984, and 1985 relative to a survey from 1975. Because leveling prior to 1975 detected little or no displacement, this survey may serve as a base for subsequent measurements. The magnitude of the uplift from 1975 to the present, coupled with strong seismic activity within the caldera, led to the conclusion that magma intrusion has taken place [*Savage and Clark*, 1982; *Savage and Cockerham*, 1984; *Rundle and Whitcomb*, 1984; *Castle et al.*, 1984]. The existance of a magma reservoir below Long Valley caldera is supported by many lines of geophysical evidence such as P wave teleseismic delays [*Steeples and Iyer*, 1976; *Ryall and Ryall*, 1981], S wave attenuation [*Sanders*, 1984; *Sanders and Ryall*, 1983], P wave tomography [*Kissling et al.*, 1984], and focal mechanisms [*Julian*, 1983].

A variety of models have been proposed to account for the observed deformation (Table 1). For example, various point source models have been proposed by *Savage and Clark*

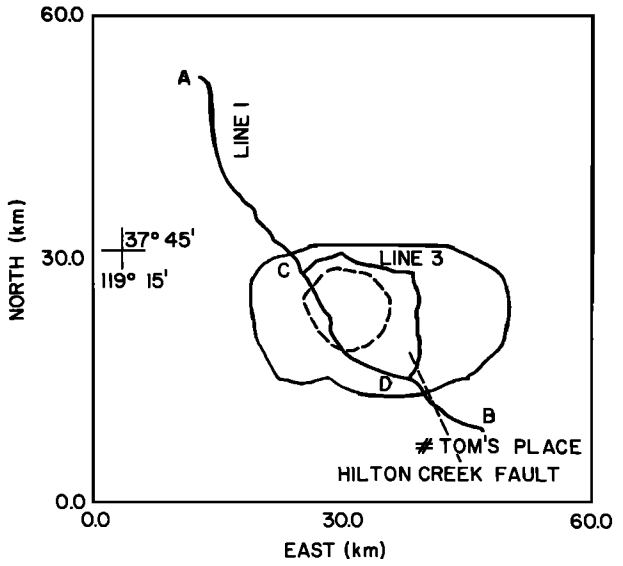

Fig. 4. Location map showing the Long Valley caldera region. The caldera is outlined by the solid oval. Leveling lines 1 and 3, measured in the base year 1975, are indicated. The Hilton Creek fault zone cuts the southern edge of the caldera and is denoted by the dashed line. The resurgent dome is indicated by a dashed circle within the caldera.

[1982], *Castle et al.* [1984], and *Rundle and Whitcomb* [1984] to explain the vertical displacement increases. Also, *Savage and Cockerham* [1984] proposed a more complicated model consisting of two dipping dikes to account for the 1975–1983 deformation. Unfortunately, surface displacement, like potential field data, does not allow the determination of a unique source model. Recently, *Wu and Wang* [1988] addressed this problem by considering a family of ellipsoidal bodies fitting the data. *Vasco* [1985] placed unique extremal bounds on the location of any magma body satisfying the data within specified error bounds for the intervals 1975–1982 and 1975–1983.

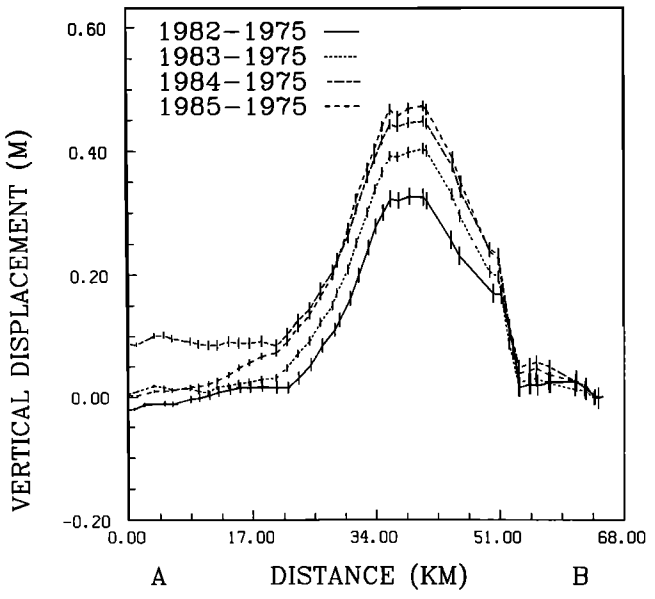

Fig. 5. Vertical displacement along Highway 395 (line 1) in Long Valley caldera for the four intervals 1982–1975, 1983–1975, 1984–1975, and 1985–1975. The distance is measured from the northwest end of the line. The vertical lines at each data point indicate the standard error of each measurement.

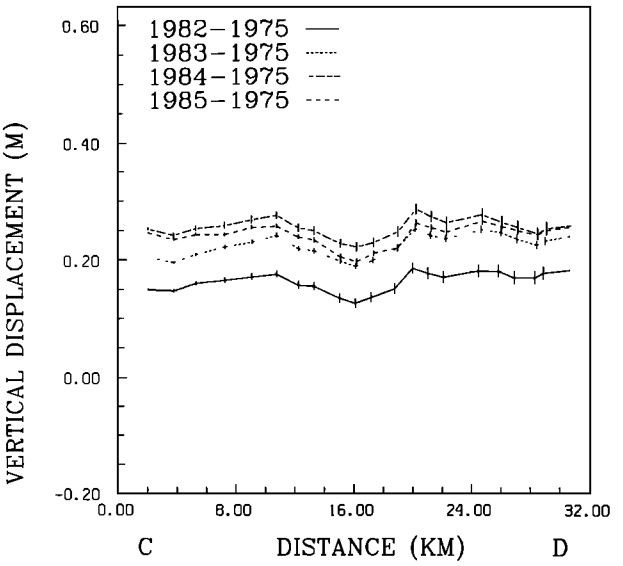

Fig. 6. Uplift and standard errors along line 3, which follows an access road circling to the north and east of the resurgent dome. The distance is from the northernmost intersection with Highway 395.

To derive a model of the possible magma intrusion in the region, we assume that the uplift is only due to volume expansion. Beginning with equation (15), we have discretized the distribution of strain nuclei using the series expansion method with respect to the rectangular constant basis functions. The requirement that the data are satisfied and that only intrusion is occurring results in a linear system of equalities and inequalities with M data points and N blocks,

$$u_i = \sum_{n=1}^{N} k_{i,n}\Delta\theta_n \qquad i = 1, 2, 3, \cdots, M \tag{16}$$

$$\Delta\theta_n \geq 0 \qquad n = 1, 2, 3, \cdots, N \tag{17}$$

Here $\Delta\theta_n$ is the fractional volume change of the nth block and u_i is the uplift at the ith station; $k_{i,n}$ is the kernal given above equation (15), integrated over the nth block. For the case under study this formulation was modified somewhat. Instead of inverting the uplift at each station we inverted the relative uplift between adjacent station pairs. This was done because the leveling measurements are correlated: the elevation at a given station depends on the elevation recorded at the preceding station. Therefore we decided to consider the difference in elevation between stations, which can be considered an independent random variable. Another advantage of this approach is that this quantity is not dependent on any constant datum shift of the measurements which occur when the base station is not stationary between surveys.

As is often the case, there are many sources of error. Two principal sources will be considered: random measurement errors and systematic errors. A major component of the errors in leveling tends to be random and are described by the formula [*Savage et al.*, 1987]

$$\sigma_i = \gamma L_i^{1/2} \tag{18}$$

where γ is a constant and L_i is the distance between the ith station pair. For the difference between two surveys, equation (18) may be used with $\gamma = 2.0$ mm/km$^{1/2}$. There are also significant sources of systematic error: rod calibration, atmospheric refraction, turning point settlement, etc. *Savage et al.*

TABLE 1. Models Derived From Various Displacement Data Sets

Reference	Interval	Chamber Model	Depth to Center, km	Volume Change, km^3
Savage and Clark [1982]	1980–1975	point source	11	0.15
Savage and Cockerham [1984]	1983–1982	dipping dike	10	0.03
Rundle and Whitcomb [1984]	1983–1975	two spheres	5, 8	0.0045, 0.05
Castle et al. [1984]	1983–1975	sphere	10	0.19
Denlinger and Riley [1984]	1982–1975	sill sphere	7–8, <7	0.019, 0.004
Wu and Wang [1988]	1982–1975	ellipsoid	9.5	0.17
Vasco [1985]	1983–1975	extremal bounds	<11	

Note the variety of time intervals and the differing models proposed. All proposed models lie above 13 km.

[1987] believe that with the exception of the 1982 and 1984 surveys, systematic errors are not significant. The 1982 survey was affected by a magnetic deflection of the level compensators used. They estimate that the maximum deviation caused by this error is only 25 mm and therefore should not seriously effect the results. However, for the 1984 survey the systematic errors seem significant, and for this reason we have chosen not to use this data.

Analysis of the three intervals 1982–1975, 1983–1975, and 1985–1975 was hampered by the few data (60 stations) for the base year 1975. This problem does not occur for 1-year intervals after 1975 such as 1983–1982, but the amount of uplift was much less during these later intervals. Given the errors associated with the surveys, the information in the other intervals may not be significant. It is seen from Figures 5 and 6 that significant vertical displacement has occurred for the interval 1985–1982. Furthermore, 117 stations were measured in those years (Figure 7). For this reason the interval was chosen to derive a model of volume expansion fitting the observed displacements. The region was discretized into four layers of thickness 4 km. Each layer was in turn divided into 25 blocks, five on each side (Figure 7) for a total of 100 unknowns. Each block is 4 km in height, 6 km in east-west width, and 5 km in north-south width for a net volume of 120 km^3.

In order to solve the system of equality and inequality constraints (equations (16) and (17)) we used the algorithm NNLS from *Lawson and Hanson* [1974, p. 158]. There was some concern over the stability of the algorithm with respect to degeneracies in the kernal matrix **k** in equation (16). Two approaches were taken to attack this problem. First, the matrix was prewhitened by adding a small amount of white noise to the matrix elements of **k**. Perturbations of 1% of the

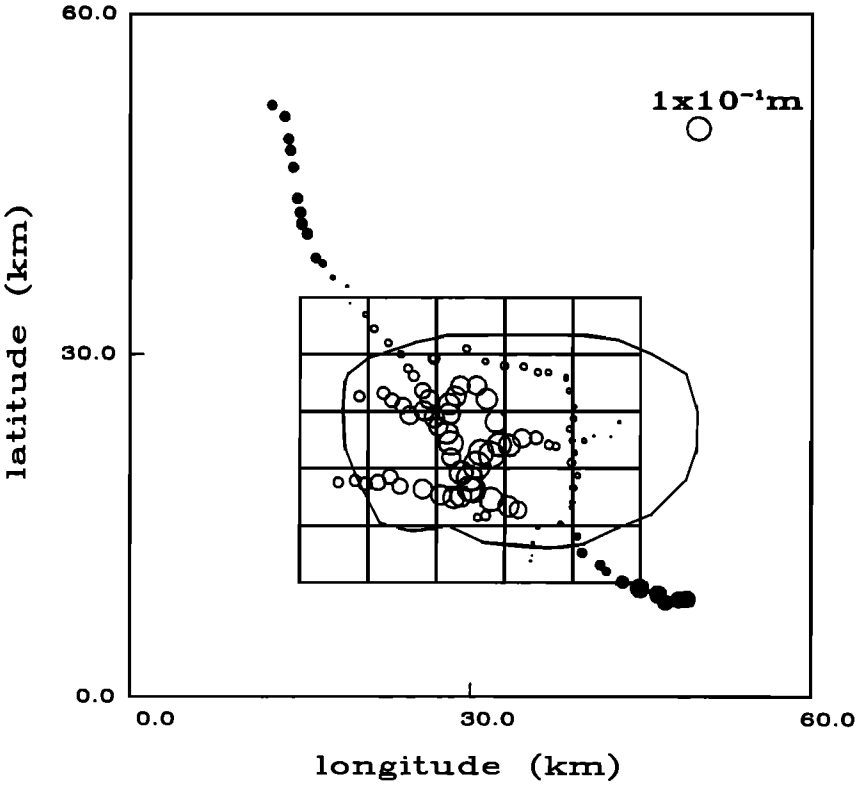

Fig. 7. Vertical displacement for the interval 1985–1982. The outline of the caldera is shown as is the horizontal discretization used in the inversion. The surface projection of the grid used in the discretization of the region is also shown. The uplift is indicated by open circles centered on the station with radii proportional to the displacement. Decreases in elevation are denoted by solid circles.

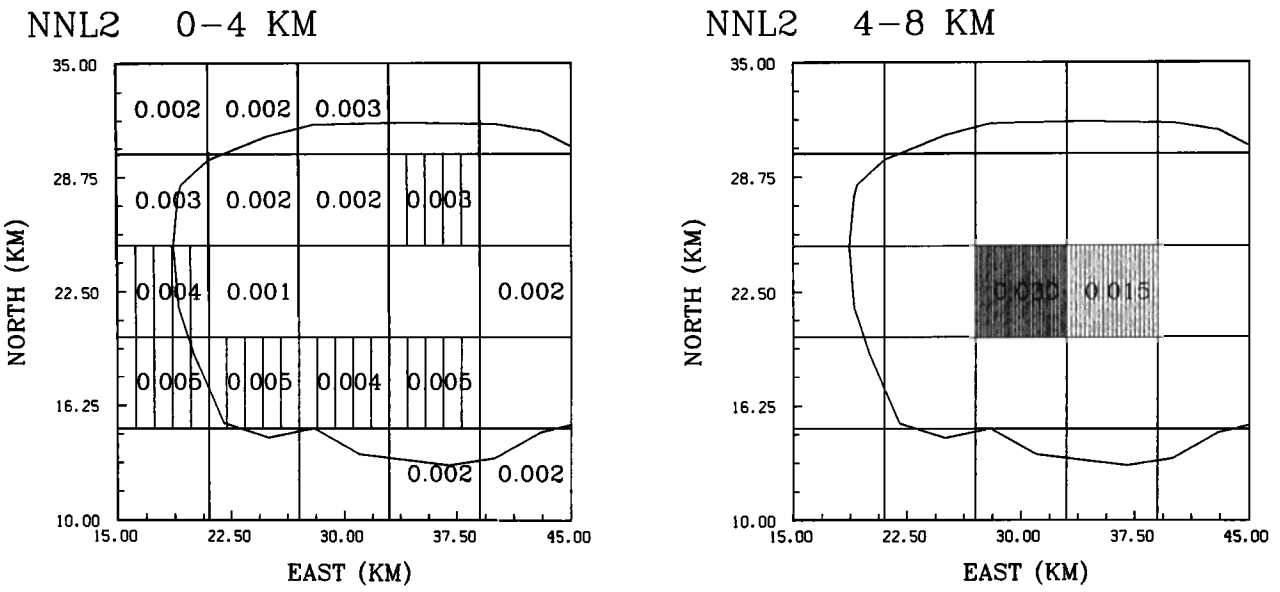

Fig. 8. Results of the nonnegative generalized inversion of the data in Figure 7. The volume expansion is in cubic kilometers. Each layer is 4 km thick. The outline of the caldera is shown by the solid line. Only the top two layers (upper 8 km) had volume expansions greater than or equal to 0.001 km^3. The largest expansion, 0.030 km^3, occurred in the 4–8 km depth range.

maximum of the elements in each row were added to the components of **k**. This eliminated some large expansion values on the periphery of the model which were suspect due to the lack of data there. Raising the percentages of prewhitening to 10% had no additional effect on the 1% solution. Second, we used a singular-valued decomposition of **k** to eliminate the small eigenvalues of the matrix and stabilize the inverse. As might be expected, this resulted in a solution (Figure 8) similar to the prewhitened solution.

We see that the largest volume expansions occur in the second layer which lies between 4 and 8 km. Here, the intrusion is concentrated in two blocks in the central caldera region which have undergone volume changes of 0.030 km^3 and 0.015 km^3. No changes are found below this layer, and only weak and diffuse expansions are found above the layer, most less than 0.005 km^3. Because of the positivity constraints, no oscillations are observed, and no contraction is present. Some caution is required in interpreting the exact location of the volume changes due to the dependence on the discretization. The discretization forces a continous distribution to become a discontinous one. A confidence interval of plus or minus one-half grid spacing should be associated with each block boundary. We note that another inversion method, the l^1 residual norm minimization with positive constraints, indicated an intrusion in the 4–8 km deep layer, also with a diameter greater than one block.

Because of the nonnegativity condition (equation (17)) the problem is no longer linear, and conventional measures of resolution and variance (equations (9) and (10)) could not be used to assess the solution. We followed the approach of *Ward and Barrientos* [1986], perturbing the data by adding normally distributed errors of the form given in equation (18) to each datum. Then the inverse was computed using the perturbed data. This was done 10,000 times, giving a population of solutions. The mean and standard error of this population were computed and these are shown in Figures 9 and 10, respectively. The mean model is strikingly similar to the unperturbed result in Figure 8. The standard error indicates that one block in the 0–4 km depth range has a significantly large confidence interval (Figure 10). In the 4–8 km range, five blocks have standard errors larger than or equal to 0.001 km^3. The two center blocks with large mean values of 0.029 and 0.014 km^3 are particularly interesting. Importantly, the standard errors (0.002 km^3) of these blocks are much smaller than their mean values. Examining a histogram of the distribution of 10,000 volume expansion values for the block undergoing the largest volume change reveals a nearly normal distribution about it's mean value of 0.029 km^3 (Figure 11). Variables with values near zero might be expected to deviate most strongly from normality due to the positivity constraint.

Positivity played a crucial role in constraining the solution. We computed a generalized inverse without the positivity constraints. Without damping or a cutoff of the small eigenvalues, the resulting solution contained large oscillations between positive and negative values. When damping was employed, the oscillations were reduced, and the minimum norm solution was produced. To reduce the solution norm, the volume expansion was concentrated in the surface layer. The addition of a positivity constraint, which is physically reasonable, gave a significantly different model in which the magma is at a greater depth.

CONCLUSIONS

The problem of determining subsurface deformations from surface displacements may be discretized through an expansion of the displacement nuclei distribution into orthonormal basis functions. The advantage of the above approach is that no source need be assumed. In some cases it may be more correct to treat a fault zone as a volume of shear rather than slip over an infinitesimal plane. Models may be found by an l^2-based inverse method or by minimizing the l^1 norm of the residuals. A more cautious approach might be to search for bounds on model parameters; these bounds may be used to characterize the range of possible solutions [*Parker*, 1972, 1974, 1975; *Sabatier*, 1977*a*, *b*].

We wish to emphasize the central role of nonlinearity in

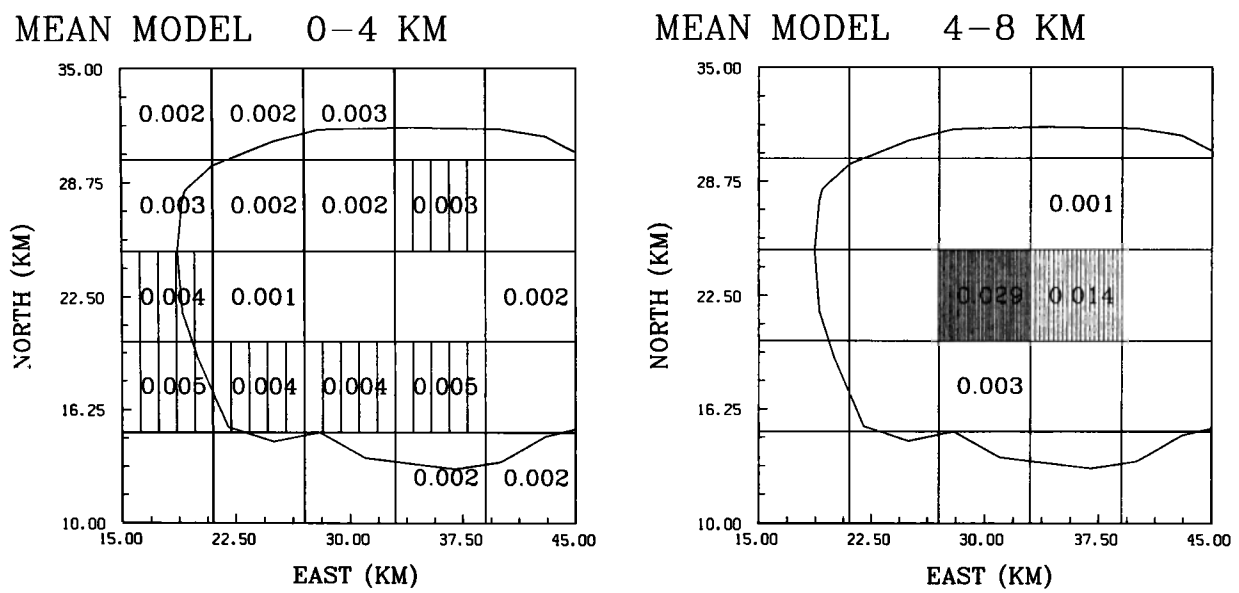

Fig. 9. The mean model of 10,000 inversion results when the data were perturbed by random errors of the form of equation (18). Again, the results are cubic kilometers. The largest expansion, 0.029 km^3,is again in the second layer.

constructing the solutions. It is only by minimizing a nonlinear functional, such as the l^1 or l^2 norm of the residuals that the models above were derived. Nonlinearity is also crucial in the computation of extremal bounds. Here it was the presence of inequalities, which are inherently nonlinear, that provided the constraints determining the solution.

Applying the numerical analysis to the uplift observed at Long Valley caldera, we calculated a model for magma intrusion there. The model contains no expansion below 8 km and a concentration of intrusion in the central portion of the caldera. This agrees with other inversions of displacement shown in Table 1. The recent inversions of *Savage et al.* [1987] result in somewhat similar conclusions. They find the predominant volume expansion (0.023 km^3) at a depth of 10 km in the south central caldera region in the 1985–1982 interval. Furthermore, after the displacement from their model is removed from the uplift, the largest residuals are found in the southwestern edge of the caldera. They indicate that either a systematic, elevation-dependent error is present or a source of uplift exists in this region. When examining our inversion result (Figure 8), we see that the largest expansions (0.005 km^3) occurring in the uppermost layer (0–4 km) is along the southern and western edges of the caldera. As noted by *Savage et al.* [1987], the west-southwest feature may represent actual shallow intrusion near Mammoth Mountain or it may be an artifact due to an elevation-dependent systematic error. The row of blocks at the southern caldera edge with volume changes of 0.005 km^3 may be due to intrusion along the south moat fault zone, as first suggested by *Savage and Cockerham* [1984]. The western half of the zone was the site of an intense swarm of earthquakes in the 1982 to 1983 interval. Intrusion within the zone of seismicity can account for much of the uplift in the area [*Savage and Cockerham*, 1984]. These considerations could be responsible for the expansion in the uppermost (0–4 km) layer in our model.

While our results are also supported by the recent tomo-

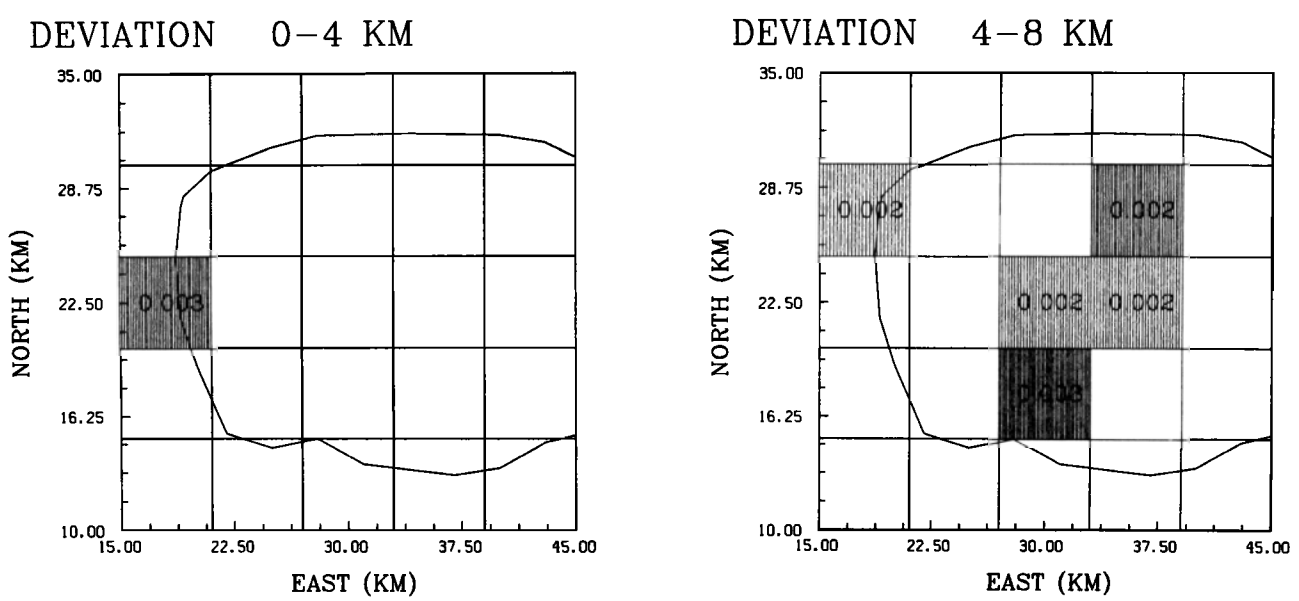

Fig. 10. The standard error of the 10,000 perturbed inversion results. The largest errors have values of 0.003 km^3.

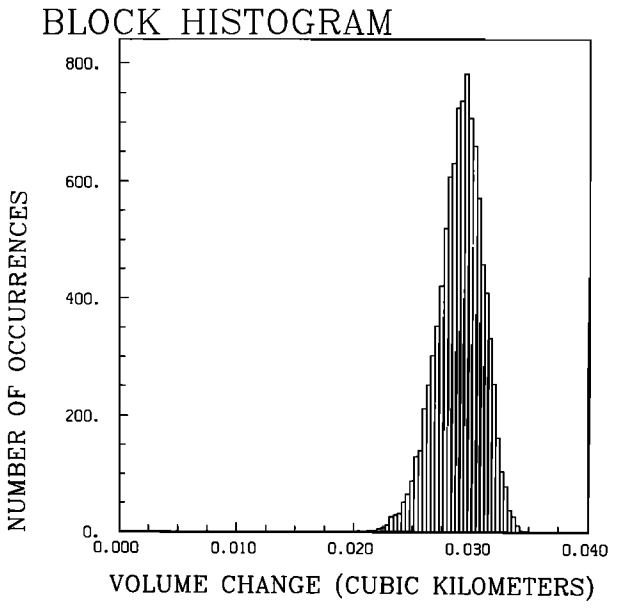

Fig. 11. A histogram of the 10,000 volume expansion values for block 48. This is the block in the 4–8 km depth range that contained the largest mean expansion value of 0.029 km^3. It's standard error is 0.002 km^3.

graphic inversions [*Kissling et al.*, 1984] in which a significant P velocity low lies above 8 km, the top of the expansion is poorly resolved by our crude discretization. Perhaps a better partition of the region would be to use blocks increasing in size with depth. The effect of faulting could easily be included in deriving the models by including the proper terms in the expansion. Even without these refinements the above method has provided reasonable results, in agreement with other methods.

Appendix

Maruyama [1964] has calculated the Green functions relating the six strain nuclei at the source ξ to the displacement at $\mathbf{x}$. This method is only for a Poisson's solid $\lambda = \mu$. To generalize this to a body with any Poisson's ratio is a matter of some algebra. Given below are the kernals for such a body when the measurements are made at the surface ($x_3 = 0$).

Without loss of generality, let the source point be at $\xi = (0, 0, \xi_3)$. Furthermore, define

$$\alpha = \frac{(\lambda + \mu)}{(\lambda + 2\mu)}$$

$$S = (x_1^2 + x_2^2 + \xi_3^2)^{1/2}$$

$$r = (x_1^2 + x_2^2)^{1/2}$$

and

$$p = \xi_3$$

Then the expressions for $W_m^{kl}(\mathbf{x}, \xi)$ are

$$W_1^{11}(\mathbf{x}, \xi) = \frac{x_1}{4\pi}\left\{2\left(1 - \frac{1}{\alpha}\right)\left[\frac{1}{r^4}\left(6p - 2S - 5\frac{p^2}{S} + \frac{p^4}{S^3}\right) - \frac{x_1^2}{r^6}\left(8p - 3S - \frac{6p^2}{S} + \frac{p^4}{S^3}\right)\right] + 6\frac{x_1^2}{S^5}\right\}$$

$$W_2^{11}(\mathbf{x}, \xi) = \frac{x_2}{4\pi}\left\{2\left(1 - \frac{1}{\alpha}\right)\left[\frac{1}{r^4}\left(2p - 3\frac{p^2}{S} + \frac{p^4}{S^3}\right) - \frac{x_1^2}{r^6}\left(8p - 3S - \frac{6p^2}{S} + \frac{p^4}{S^3}\right)\right] + 6\frac{x_1^2}{S^5}\right\}$$

$$W_3^{11}(\mathbf{x}, \xi) = \frac{1}{4\pi}\left\{2\left(1 - \frac{1}{\alpha}\right)\left[\frac{1}{r^2}\left(1 - 2\frac{p}{S} + \frac{p^3}{S^3}\right) - \frac{x_1^2}{r^4}\left(2 - 3\frac{p}{S} + \frac{p^3}{S^3}\right)\right] - 6\xi_3\frac{x_1^2}{S^5}\right\}$$

$$W_1^{12}(\mathbf{x}, \xi) = \frac{x_2}{4\pi}\left\{2\left(1 - \frac{1}{\alpha}\right)\left[\frac{1}{r^4}\left(2p - S - \frac{p^2}{S}\right) - \frac{x_1^2}{r^6}\left(8p - 3S - \frac{6p^2}{S} + \frac{p^4}{S^3}\right)\right] + 6\frac{x_1^2}{S^5}\right\}$$

$$W_2^{12}(\mathbf{x}, \xi) = \frac{x_1}{4\pi}\left\{2\left(1 - \frac{1}{\alpha}\right)\left[\frac{1}{r^4}\left(2p - S - \frac{p^2}{S}\right) - \frac{x_2^2}{r^6}\left(8p - 3S - \frac{6p^2}{S} + \frac{p^4}{S^3}\right)\right] + 6\frac{x_2^2}{S^5}\right\}$$

$$W_3^{12}(\mathbf{x}, \xi) = \frac{x_1 x_2}{4\pi}\left\{2\left(1 - \frac{1}{\alpha}\right)\frac{1}{r^4}\left(-2 + 3\frac{p}{S} - \frac{p^3}{S^3}\right) - \frac{6\xi_3}{S^5}\right\}$$

$$W_1^{13}(\mathbf{x}, \xi) = \frac{1}{4\pi}\left\{-6x_1^2\frac{\xi_3}{S^5}\right\}$$

$$W_2^{13}(\mathbf{x}, \xi) = \frac{1}{4\pi}\left\{-6x_1x_2\frac{\xi_3}{S^5}\right\}$$

$$W_3^{13}(\mathbf{x}, \xi) = \frac{1}{4\pi}\left\{6x_1\frac{\xi_3^2}{S^5}\right\}$$

$$W_1^{33}(\mathbf{x}, \xi) = \frac{x_1}{4\pi}\left\{6\frac{\xi_3^2}{S^5}\right\}$$

$$W_2^{33}(\mathbf{x}, \xi) = \frac{x_2}{4\pi}\left\{6\frac{\xi_3^2}{S^5}\right\}$$

$$W_3^{33}(\mathbf{x}, \xi) = \frac{1}{4\pi}\left\{-6\frac{\xi_3^3}{S^5}\right\}$$

The expressions for $W_m^{22}(\mathbf{x}, \xi)$ can be derived from the $W_m^{11}(\mathbf{x}, \xi)$ terms by interchanging x_1 and x_2. Similarly, the kernals $W_m^{23}(\mathbf{x}, \xi)$ are found from W_m^{13} by interchanging x_1 with x_2 and ξ_1 with ξ_2.

Acknowledgments. We wish to thank J. C. Savage for supplying the data as well as some useful suggestions. This report was supported by the Assistant Secretary for Renewable Energy, Division of Geothermal Technology and the Office of Energy Research, Office of Basic Energy Sciences, Division of Engineering and Geosciences, U.S. Department of Energy under contract DE-AC03-76SF00098. Center for Computational Seismology contribution 43.

References

Aki, K., and P. G. Richards, *Quantitative Seismology Theory and Methods*, vol. I, W. H. Freeman, San Francisco, Calif., 1980*a*.

Aki, K., and P. G. Richards, *Quantitative Seismology Theory and Methods*, vol. II, W. H. Freeman, San Francisco, Calif., 1980*b*.

Backus, G. E., and J. F. Gilbert, The resolving power of gross earth data, *Geophys. J. R. Astron. Soc.*, *16*, 169–205, 1968.

Castle, R. O., J. E. Estrem, and J. C. Savage, Uplift across Long Valley caldera, California, *J. Geophys. Res.*, *89*, 11,507–11,515, 1984.

Dantzig, G. B., *Linear Programming and Extensions*, Princeton University Press, Princeton, N. J., 1963.

Denlinger, R. P., and F. S. Riley, Deformation of Long Valley caldera, Mono County, California, from 1975 to 1982, *J. Geophys. Res.*, *89*, 8304–8314, 1984.

Dieterich, J. H., and R. W. Decker, Finite element modeling of surface deformation associated with volcanism, *J. Geophys. Res.*, *80*, 4094–4102, 1975.

Eshelby, J. D., The determination of the elastic field of an ellipsoidal inclusion, and related problems, *Proc. R. Soc. London, Ser. A*, *241*, 376–396, 1957.

Hadley, G., *Linear Programming*, Addison-Wesley, Reading, Mass., 1962.

Jovanovich, D. B., M. I. Husseini, and M. A. Chinnery, Elastic dislocations in a layered half-space, I, Basic theory and numerical methods, *Geophys. J. R. Astron. Soc.*, *39*, 205–217, 1974.

Julian, B. R., Evidence for dyke intrusion earthquake mechanisms near Long Valley caldera, California, *Nature*, *303*, 323–324, 1983.

Kissling, E., W. Ellsworth, and R. S. Cockerham, Three-dimensional structure of the Long Valley caldera, California, region by geotomography, *U.S. Geol. Surv. Open File Rep.*, *84-939*, 188–220, 1984.

Langbein, J. O., An interpretation of episodic slip on the Calaveras fault near Hollister, California, *J. Geophys. Res.*, *86*, 4941–4948, 1981.

Lawson, C. L., and R. J. Hanson, *Solving Least Squares Problems*, Prentice-Hall, Englewood Cliffs, N. J., 1974.

Madariaga, R., Earthquake source theory: A review, *Proc. Int. Sch. Phys. Enrico Fermi*, *85*, 1–44, 1983.

Maruyama, T., Statical elastic dislocations in an infinite and semi-infinite medium, *Bull. Earthquake Prev. Res. Inst. Univ. Tokyo*, *42*, 289–368, 1964.

Menke, W., *Geophysical Data Analysis: Discrete Inverse Theory*, Academic, Orlando, Fla., 1984.

Parker, R. L., Inverse theory with Grossly inadequate data, *Geophys. J. R. Astron. Soc.*, *29*, 123–138, 1972.

Parker, R. L., Best bounds on density and depth from gravity data, *Geophysics*, *39*, 644–649, 1974.

Parker, R. L., The theory of ideal bodies for gravity interpretation, *Geophys. J. R. Astron. Soc.*, *42*, 315–334, 1975.

Rundle, J. B., and J. H. Whitcomb, A model for deformation in Long Valley, California, 1980–1983, *J. Geophys. Res.*, *89*, 9371–9380, 1984.

Ryall, F., and A. Ryall, Attenuation of *P* and *S* waves in a magma chamber in Long Valley caldera, California, *Geophys. Res. Lett.*, *8*, 557–560, 1981.

Sabatier, P. C., Positivity constraints in linear inverse problems, I, General theory, *Geophys. J. R. Astron. Soc.*, *48*, 415–441, 1977*a*.

Sabatier, P. C., Positivity constraints in linear inverse problems, II, Applications, *Geophys. J. R. Astron. Soc.*, *48*, 443–459, 1977*b*.

Sanders, C. O., Location and configuration of magma bodies beneath Long Valley, California, determined from anomalous earthquake signals, *J. Geophys. Res.*, *89*, 8287–8302, 1984.

Sanders, C. O., and F. Ryall, Geometry of magma bodies beneath Long Valley, determined from anomalous earthquake signals, *Geophys. Res. Lett.*, *10*, 690–692, 1983.

Savage, J. C., and M. M. Clark, Magmatic resurgence in Long Valley caldera, California: Possible cause of the 1980 Mammoth Lakes earthquakes, *Science*, *217*, 531–533, 1982.

Savage, J. C., and R. S. Cockerham, Earthquake swarm in Long Valley caldera, California, January 1983: Evidence for dike inflation, *J. Geophys. Res.*, *89*, 8315–8324, 1984.

Savage, J. C., W. H. Prescott, and G. Gu, Strain accumulation in southern California, 1973–1984, *J. Geophys. Res.*, *91*, 7455–7473, 1986.

Savage, J. C., R. S. Cockerham, J. E. Estrem, and L. R. Moore, Deformation near the Long Valley caldera, eastern California, 1982–1986, *J. Geophys. Res.*, *92*, 2721–2746, 1987.

Segall, P., and R. Harris, Earthquake deformation cycle on the San Andreas fault near Parkfield, California, *J. Geophys. Res.*, *92*, 10,511–10,525, 1987.

Steeples, D. W., and H. M. Iyer, Low-velocity zone under Long Valley as determined from teleseismic events, *J. Geophys. Res.*, *81*, 849–860, 1976.

Tarantola, A., and B. Valette, Generalized nonlinear inverse problems solved using the least squares criterion, *Rev. Geophys.*, *20*, 219–232, 1982.

Vasco, D. W., Extremal inversion of vertical displacements, Long Valley caldera, California 1982/1983, *J. Geophys.*, *57*, 178–183, 1985.

Vasco, D. W., Inversion of static displacement of the Earth's surface, Ph.D. thesis, Univ. of Calif., Berkeley, 1986.

Vasco, D. W., and L. R. Johnson, Extremal inversion of static Earth displacements due to volume sources, *Geophys. J. R. Astron. Soc.*, *80*, 223–239, 1985.

Volterra, V., Sur l'equilibre des corps elastiques multiplement connexes, *Ann. Sci. Ecole Norm. Super. Paris*, *24*, 401–517, 1907.

Ward, S. N., and S. E. Barrientos, An inversion for slip distribution and fault shape from geodetic observations of the 1983, Borah Peak, Idaho, earthquake, *J. Geophys. Res.*, *91*, 4909–4919, 1986.

Wiggins, R A., The general linear inverse problem: Implication of surface waves and free oscillations for earth structure, *Rev. Geophys.*, *10*, 251–285, 1972.

Wu, M., and H. F. Wang, Deformations and inferred stress field sensitivity for ellipsoidal sources at Long Valley, California, 1975–1982, *J. Geophys. Res.*, in press, 1988.

N. E. Goldstein and L. R. Johnson, Center for Computational Seismology, Earth Sciences Division, Lawrence Berkeley Laboratory, University of California, Berkeley, CA 94720.

D. W. Vasco, Earth Sciences Division, Air Force Geophysics Laboratory/LWG, Hanscom Air Force Base, MA 01731.

(Received April 22, 1987;
revised November 16, 1987;
accepted November 16, 1987.)